

**EVOLUTION OF HYDRO-CLIMATOLOGICAL  
EXTREMES AND MODELLING OF ASSOCIATED  
NON-STATIONARITY**

**VINNARASI RAJENDRAN**



**DEPARTMENT OF CIVIL ENGINEERING  
INDIAN INSTITUTE OF TECHNOLOGY DELHI  
OCTOBER 2019**

© Indian Institute of Technology Delhi (IITD), New Delhi, 2019

**EVOLUTION OF HYDRO-CLIMATOLOGICAL EXTREMES AND  
MODELLING OF ASSOCIATED NON-STATIONARITY**

*by*

**VINNARASI RAJENDRAN**

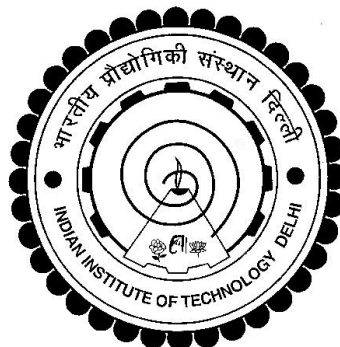
Department of Civil Engineering

*Submitted*

*in fulfillment of the requirements for the degree of Doctor of*

*Philosophy*

*to the*



**INDIAN INSTITUTE OF TECHNOLOGY DELHI  
JUNE 2019**

## CERTIFICATE

This is to certify that the dissertation entitled “**Evolution of Hydro-climatological Extremes and Modelling of Associated Non-Stationarity**” which is being submitted by **Mrs. Vinnarasi Rajendran**, for the award of the degree of **Doctor of Philosophy** in Civil Engineering, to the Indian Institute of Technology Delhi is a record of bona fide work carried out by her under my sustained guidance and supervision. The dissertation has reached the standard fulfilling the requirements of the regulations relating to the degree. The results embodied in the dissertation have not been submitted to any other university or institute for the award of any degree or diploma.

**Prof. Dhanya C. T.**

Associate Professor

Department of Civil Engineering

Indian Institute of Technology Delhi

New Delhi - 110016

## ACKNOWLEDGMENTS

I thank the almighty God in the first place for His guidance and revelations in every aspect of this thesis. I thank Him, especially for giving Prof. Dhanya as my supervisor and for providing all the necessary things to carry out this work. I want to express my sincere thanks to **Prof. Dhanya** and feel privileged to be her student, who taught me to explore and learn independently. Her commendable dedication towards research, unconditional support, and valuable guidance helped me to push forward throughout my Ph. D. I am grateful to her for the continuous support and immense time she gave me, which helped to enhance the quality of this thesis and publish articles in reputed journals.

I want to thank the Head, Department of Civil Engineering, Indian Institute of Technology Delhi, for providing a conducive environment for research. It is a pleasure to thank my SRC (Student Research Committee) members – Prof. A. K. Gosain, Prof. Krishna AchutaRao, and Prof. K.S. Rao – for their valuable suggestions during this Ph. D. journey. I would also like to thank all the faculties and staff of Department of Civil Engineering, IIT Delhi, especially, Mr. N. R. Gehlot and Mr. Rajveer Aggarwal.

I am indebted to Jennifer and Renuka for their love and care during my hospitalization, amid their research work. I thank my study group – Ms. Ponni and Mrs. Chitra – for their discussion during my course work, which helped me to learn the subjects in depth. I want to thank all the members of HydroX Research Group, especially Dr. Pawan, Dr. Aniket, Shushobhit, and Nikhil, for their valuable advice and guidance. Besides, Shushobhit and Nikhil, more than being my colleagues, became my brothers, having many discussions, fun, and hangouts. I would also thank Dinesh Kumar, Ishita Bhatnagar, Archana Majhi, and Sudeep for helping in arranging and proofreading the thesis. I would also extend my thanks to my lab mates – Nitesh Patidar, Gopinadh Rongali, Himanshu, and Khwairakpam Eliza for their support and help.

I thank my parents for all their sacrifices and encouragement. Without them, I would not have reached this far. Especially in the final stage of my Ph. D., they helped and supported me in all the ways to complete this work. I thank my husband for being patient and supportive throughout the journey of Ph. D. I thank my sister Vennila for

taking care of my daughter and helping me in various other aspects of the Ph. D. I thank my parents-in-law for their consistent prayer and moral support. I also offer special thanks to my sister-in-law's family, James, and Ruby for their encouraging words and continuous support, especially to Jerusha James, who prayed for my Ph. D. work

I especially thank my spiritual parents Mr. & Mrs. Joseph; Mr. & Mrs. Sam Israel, Mrs. Joy Josaiiah and Mrs. Rebecca Daniel, who guided and counseled me, in every walk of my life, to keep the peace in my heart during failures and discouragements. I would also like to thank my Church in Delhi for backing me up with love and prayer during tough times, especially Mr. Amal Fraser, Mr. & Mrs. Joshua Moody, Mr. & Mrs. Aldrin Joseph, Mr. & Mrs. Amose, Mr. & Mrs. Santhosh, Mr. & Mrs. Rosy, Ezekiel Paul, Chilly, Anusha, and Ms. Mercy Rao. I thank my brothers and sisters from IIT Fellowship, especially Prasad Anna, Mary, Pujitha, Joicy, Ashish, Joshua, and Karundeep, for praying with me and sharing in all my joys and sorrows. Moreover, they took care of me like their family member during my pregnancy and delivery. Chilly, Ezekiel Paul and Pujitha gave their laptop for my work.

I want to express my sincere gratitude to my masters' supervisor, Prof. Arup Kumar Sarma, who introduced me to the world of climate change and encouraged me to pursue Ph. D. I want to thank Prof. Amir AghaKouchak for valuable advice and constructive comments on the collaborative paper. Special thanks to Dr. Aniket Chakravorthy, who shared his knowledge of atmospheric science; Mr. Hemant Kumar, who assisted me in writing MATLAB codes for Chapter 7; Shushobit, Ashish and Joshua, who helped me to format the plots.

Finally, I thank my daughter Hannah Christy, a heritage from God, who kept us cheerful and enthusiastic. Without her cooperation, I would not have completed this thesis. It would take a lot of space to recount all the people who contributed in some way or the other to this thesis. I thank all the people who have impacted my life.

**Vinnarasi Rajendran**  
Research Scholar  
Department of Civil Engineering  
Indian Institute of Technology Delhi  
New Delhi - 110016

## ABSTRACT

Modeling of extreme events and their dynamic behavior has always been an interesting and challenging topic. Increase in the magnitude and frequency of extreme hydro-climatological events have been widely reported in recent decades, which are generally attributed to the recent revelation of abrupt changes in climate. Moreover, it poses great threat to the sustainability of the existing water resources systems and infrastructure, which are usually designed using the traditional ‘stationarity’ assumption, i.e., the statistical properties of extreme events are time invariant. Therefore, to tackle the adverse consequence arising from the changing climate, a robust methodology needs to be developed by incorporating the temporal dynamics into multivariate extreme event modeling. Before estimating the hydrologic variable for design and maintenance of water resources infrastructure, it is essential to fathom the historical changes and trends. To achieve this, three broad objectives are enumerated: 1. Re-examine the changing characteristics of hydro-climatological extremes over India, 2. Explore the effect of non-stationarity and interdependency in the multivariate non-stationary extreme event modeling, and 3. Investigate the suitable climate-informed covariate in order to assess the impact of climate change on extreme precipitation.

The first aim of this research is to analyze the spatio-temporal variations and trends in the extreme (wet and dry spells) Indian monsoon precipitation, using  $0.25^{\circ}\times 0.25^{\circ}$  high resolution gridded data for 113 years (1901-2013). Significant increase in the maximum intensity of rainfall and spatial heterogeneity is observed over the past half-century. Besides, significant negative trends in wet spell durations and positive trends in dry spell durations are observed over wet regions; whereas contrasting trends are observed over dry regions. A shift in the frequency distribution of extreme events during the monsoon period is also noticed. The 50 year return level of maximum intensity clearly shows positive trends over the past century. Though characteristics of extremes are observed to be highly localized, apparent signs of wet regions turning drier and dry regions turning wetter are noticed. A comprehensive insight into different characteristics (intensity, spell, onset, and frequency) of Indian monsoon extremes is necessary, which will help in effective water resources management and flood/drought hazard preparedness.

Further, the regional evolution of Diurnal Temperature Range (DTR) trend over different climatic zones in India is investigated using a non-linear approach known as the Multidimensional Ensemble Empirical Mode Decomposition (MEEMD) method, to explore the generalized influence of regional climate on DTR, if any. An increase of  $0.36^{\circ}\text{C}$  in the overall mean of DTR until 1980 is observed; however, the rate has declined subsequently. Further, arid deserts and warm-temperate grasslands exhibit negative DTR trends, while the west coast and sub-tropical forest in the north-east show positive trends. This transition predominantly begins with a  $0.5^{\circ}\text{C}$  increase from the west coast and spreads with an increase of  $0.25^{\circ}\text{C}$  per decade, which is more pronounced during winter and post-monsoon. Notably, in the arid desert and warm-temperate grasslands, the DTR has decreased up to  $2^{\circ}\text{C}$ , where the rate of increase in minimum temperature is higher than the maximum temperature. By and large, both maximum and minimum temperature increase in response to the global climate change; however, their rates of increase are highly local and depend on the particular climatic zone.

These observed significant changes in climate are known to have a significant impact on crop production and human resources, which are generally difficult to quantify. Hence, two new indices are defined: (i) refined growing season (GS) characteristics and (ii) transition period, based on the annual cycles of diurnal temperature extremes, to unravel any possible impact of the changing climate on these productive elements. MEEMD is used to extract the annual cycles of diurnal temperature extremes. Results reveal earlier onset and lengthening of GS, with notable spatial variations. Further, a drastic reduction in the transition (i.e., comfortable) period is observed over the warm humid regions, majorly due to the encroachment by summer days. On the contrary, over semi-arid regions, the transition period is found to be increasing, majorly due to the shortening of winter.

The observed changes in the hydro-climatological extremes further reinforce the need for nonstationary modeling to capture the dynamic behavior of the changing climate. Hence, a realistic and efficient framework to detect non-stationarity in the observed hydrologic variables, termed as Time Sliding Window (TSW) approach, is proposed to overcome some of the limitations suffered by the traditional non-stationary approaches. The proposed TSW based non-stationary modeling (TSW-NSM) is proved to be superior to traditional non-stationary model and stationary model and is employed for two applications: 1) develop joint intensity and duration relationship and 2) develop drought index.

The intensity of the rainfall is reportedly increasing, accompanied by sharp changes in the pattern of rainfall. Since direct runoff is influenced by the intensity and duration of rainfall, it is crucial to study the joint characteristics of intensity and duration in the context of non-stationarity, especially in urban regions where the relationship is more distinct. Hence, the time-varying multivariate probability frequency analysis is implemented to derive the time-varying Intensity-Duration relationship. Bayesian approach through Differential Evolution Markov Chain (DE-MC) algorithm is employed to estimate the uncertainty bound of the time-varying return level. The results emphasize that the probabilistic distribution parameters vary both temporally and spatially and recommend the incorporation of non-stationarity in the extreme event modeling if there is a change in the probabilistic distribution parameters. This non-stationary model can be seamlessly employed to compute return levels with better accuracy and reliability than traditional stationary/nonstationary methods. Results show that the short duration return level increases at a faster rate than the longer ones, with the credibility interval larger than that of long duration return levels. The results also highlight the importance of adopting event based non-stationary IDF curves for the design of water resource systems and devising long-term decision-making strategies to address the effects of changing climate.

Recent literature on drought emphasizes the need for developing a drought index incorporating the dynamic behavior of the drought characteristics. Hence, a multi-variate non-stationary drought index, termed as Non-stationary Joint Deficit Index (NJDI), is developed to capture the temporal dynamics of the hydrological variables and to identify the meteorological drought-prone areas over India. The changes observed in the distribution parameter of rainfall series emphasize an increasing number of dry days in recent decades all over India, except northeast. The comparison of NJDI and stationary Joint Deficit Index (JDI) reveals that JDI overestimates drought when frequent severe dry events are clustered and vice versa. It clearly shows that the traditional indices are biased by the lowest magnitude of precipitation. Additionally, the spatial variations of historical drought assessment of NJDI and JDI clearly depict that in the majority of regions, JDI underestimated drought in the early 19<sup>th</sup> century and overestimated the same in the later part of the century, which is in harmony with changes in the pattern of dry events over India, whereas, NJDI captured the historical drought reflecting the temporal dynamics of rainfall series and is more reliable than traditional drought indices. The proposed NJDI is found to be a potential index for drought monitoring in a nonstationary climate.

Finally, the proposed TSW-NSM is further improved by adopting climate variables as a covariate. Recent studies have questioned the suitability of time as a covariate and emphasized the possibility of improving the accuracy of the model by incorporating climate-informed covariates. Five potential climate-informed covariates have been chosen to model nonstationary annual maximum rainfall and intensity series. The changes in the distribution parameters are detected using TSW, and 32 combinations of models are developed. Further, Bayesian Differential Evolutionary Monte Carlo (DE-MC) algorithm is employed to estimate the uncertainty bounds of the non-stationary parameters, and the best model is chosen using the Deviance Information Criterion (DIC). It reveals that short duration intensity events are more influenced by local processes (i.e., local temperature changes and diurnal temperature changes), whereas longer duration intensity events are influenced by global processes (global warming and teleconnections). However, the acceptable non-stationary models reveal that the temperature-based covariates, i.e., local, diurnal, and global temperature changes, have always been good in capturing the dynamic behavior. It is also observed that the local processes carry the signature of global processes. Further, the return level computed through best non-stationary model shows that the return periods are decreasing, and short duration events have undergone drastic changes than longer duration events. Further, it is necessary to adopt climate-informed covariates based nonstationary modeling for devising long-term strategies to address the effects of changing climate.

It is expected that the quantification of the historical changes in precipitation and temperature over India may aid in implementing regional adaptation strategies. The proposed framework of multivariate nonstationary extreme event modeling is not only limited to the applications mentioned in this study. It is generic and can be employed to any climate modeling which exhibits the signature of non-stationarity.

## सार

चरम घटनाओं का प्रतिरूपण और उनका गतिशील व्यवहार हमेशा एक दिलचस्प और चुनौतिपूर्व विषय रहा है। हाल के दशकों में चरम जलविज्ञान एवं जलवायु संबंधित घटनाओं के परिमाण और आवृत्ति में व्यापक वृद्धि की आख्या कि गई है, जिसके लिए सामान्य तौर पर हाल ही में आये जलवायु में अचानक बदलाव के रहस्योद्घाटन को जिम्मेदार ठहराया गया। इसके अलावा, इससे मौजूदा जल संसाधन प्रणाली और बुनियादी ढांचे की स्थिरता को बहुत खतरा है, जो आम तौर पर स्थिर धारणा का उपयोग करके बनाया गया है, जिसके अनुसार चरम घटनाओं के संख्यिक गुण समय पर आश्रित नहीं है। इसलिए बदलती जलवायु के परिणामस्वरूप उत्पन्न होने वाले प्रतिकूल परिणाम से निपटने के लिए गैर व्यापकता को मल्टी वेरियेट चरम घटना प्रतिरूपण में शामिल कर के एक मजबूत कार्यप्रणाली विकसित करने की आवश्यकता है। जल संसाधन अवसंरचना के रचना और रखरखाव के लिए जल विग्यान सम्बन्धित चर का अनुमान लगाने से पहले, ऐतिहासिक परिवर्तनों और रुझानों को थाह लेना आवश्यक है। इसे प्राप्त करने के लिए, तीन व्यापक उद्देश्यों की गणना की जाती है: 1. भारत में पनबिजली-चरम सीमाओं की बदलती विशेषताओं की पुनः जांच करना, 2. बहुभिन्नरूपी गैर-स्थैतिक चरम घटना मॉडलिंग में गैर-स्थिरता और अन्योन्याश्रयता के प्रभाव की खोज करना, और 3। चरम वर्षा पर जलवायु परिवर्तन के प्रभाव का आकलन करने के लिए उपयुक्त जलवायु-सूचित कोवरिएट की जांच करें।

इस शोध का पहला उद्देश्य 113 वर्षों (1901-2013) के लिए  $0.25^\circ \times 0.25$  resolution उच्च रिज़ॉल्यूशन वाले ग्रिड डेटा का उपयोग करते हुए भारतीय मानसून वर्षा के चरम (गीले और सूखे मंत्र) में अनुपातिक लौकिक विविधताओं और रुझानों का विश्लेषण करना है। पिछली आधी सदी में वर्षा की अधिकतम तीव्रता और स्थानिक विषमता में उल्लेखनीय वृद्धि देखी गई है। इसके अलावा, गीले वर्तनी अवधि में महत्वपूर्ण नकारात्मक रुझान और सूखे क्षेत्रों में सकारात्मक रुझान गीले क्षेत्रों पर मनाया जाता है; जबकि इसके विपरीत रुझान शुष्क क्षेत्रों में देखे जाते हैं। मानसून अवधि के दौरान चरम घटनाओं के आवृत्ति वितरण में बदलाव भी देखा जाता है। अधिकतम तीव्रता का 50 साल का वापसी स्तर स्पष्ट रूप से पिछली शताब्दी में सकारात्मक रुझान दिखाता है। हालांकि चरम सीमाओं की विशेषताओं को अत्यधिक स्थानीयकृत किया जाता है, गीले क्षेत्रों में सुखाने वाले और सूखे क्षेत्रों को गीला करने वाले क्षेत्रों के स्पष्ट संकेत देखे जाते हैं। भारतीय मानसून चरम सीमाओं की विभिन्न विशेषताओं (तीव्रता, वर्तनी, शुरुआत, और आवृत्ति) में एक

व्यापक अंतर्दृष्टि आवश्यक है, जो प्रभावी जल संसाधन प्रबंधन और बाढ़ / सूखा खतरे की तैयारी में मदद करेगी।

इसके अलावा, भारत में विभिन्न जलवायु क्षेत्रों पर ड्यूरेनल टेम्परेचर रेंज (DTR) ट्रेंड के क्षेत्रीय विकास की जाँच DTR पर क्षेत्रीय जलवायु के सामान्यीकृत प्रभाव का पता लगाने के लिए बहुआयामी एनसेम्बल एम्पिरिकल मोड डिकम्पोजिशन (MEEMD) विधि के रूप में जाना जाता है। 1980 तक DTR के समग्र अर्थ में 0.36 °C की वृद्धि देखी गई; हालांकि, बाद में दर में गिरावट आई है। इसके अलावा, शुष्क रेगिस्तान और गर्म-शीतोष्ण घास के मैदान नकारात्मक DTR प्रवृत्तियों को प्रदर्शित करते हैं, जबकि पश्चिम-तट और उत्तर-पूर्व में उप-उष्णकटिबंधीय जंगल सकारात्मक रुझान दिखाते हैं। यह संक्रमण मुख्य रूप से पश्चिमी तट से 0.5° C की वृद्धि के साथ शुरू होता है और प्रति दशक 0.25° C की वृद्धि के साथ फैलता है, जो सर्दियों और मानसून के बाद अधिक स्पष्ट होता है। विशेष रूप से, शुष्क रेगिस्तान और गर्म-शीतोष्ण घास के मैदानों में, DTR 2° C तक कम हो गया है, जहां न्यूनतम तापमान में वृद्धि की दर अधिकतम तापमान से अधिक है। वैश्विक जलवायु परिवर्तन की प्रतिक्रिया में अधिकतम और न्यूनतम तापमान में वृद्धि से बड़े और बड़े दोनों; हालांकि, उनकी वृद्धि की दर अत्यधिक स्थानीय है और विशेष जलवायु क्षेत्र पर निर्भर करती है।

जलवायु में इन महत्वपूर्ण परिवर्तनों का फसल उत्पादन और मानव संसाधनों पर महत्वपूर्ण प्रभाव पड़ता है, जिन्हें आमतौर पर निर्धारित करना मुश्किल होता है। इसलिए, दो नए सूचकांक परिभाषित किए गए हैं: (i) परिष्कृत मौसम (जीएस) विशेषताओं और (ii) संक्रमण काल, जो कि इन उत्पादक तत्वों पर बदलते जलवायु के किसी भी संभावित प्रभाव को उजागर करने के लिए, पूर्ण तापमान के वार्षिक चक्रों पर आधारित है। MEEMD का उपयोग डायरेनल तापमान चरम सीमा के वार्षिक चक्रों को निकालने के लिए किया जाता है। परिणाम पूर्ववर्ती शुरुआत और जीएस की लंबाई को उल्लेखनीय स्थानिक बदलाव के साथ प्रकट करते हैं। इसके अलावा, संक्रमण (यानी, आरामदायक) अवधि में भारी कमी गर्म आर्द्र क्षेत्रों पर देखी जाती है, प्रमुखतः गर्मियों के दिनों में अतिक्रमण के कारण। इसके विपरीत, अर्ध-शुष्क क्षेत्रों में, संक्रमण की अवधि बढ़ती हुई पाई जाती है, जिसका मुख्य कारण सर्दियों का छोटा होना है।

हाइड्रो-क्लाइमेटोलॉजिकल चरम में देखे गए परिवर्तन गैर-संसदीय मॉडलिंग की आवश्यकता को बदलते हुए जलवायु के गतिशील व्यवहार को पकड़ने के लिए और अधिक सुदृढ़ करते हैं। इसलिए, टाइम स्लाइडिङ विन्डो (TSW) दृष्टिकोण के रूप में कहा जाता है, देखे गये हाइड्रोलॉजिक चरम में गैर-स्थिरता का पता लगाने के लिए एक यथार्थवादी और कुशल रूपरेखा, पारंपरिक गैर-स्थिर दृष्टिकोण द्वारा सामना की गई कुछ सीमाओं को दूर करने के लिए प्रस्तावित है। प्रस्तावित TSW आधारित गैर-स्थिर मॉडलिंग (TSW-

NSM) पारंपरिक गैर-स्थिर मॉडल और स्थिर मॉडल से बेहतर साबित होता है और दो अनुप्रयोगों के लिए नियोजित किया जाता है: 1) संयुक्त तीव्रता और अवधि संबंध विकसित करते हैं और 2) सूखा सूचकांक विकसित करते हैं।

कथित तौर पर वर्षा के पैटर्न में तेज बदलाव के साथ वर्षा की तीव्रता बढ़ रही है। चूंकि प्रत्यक्ष अपवाह वर्षा की तीव्रता और अवधि से प्रभावित होता है, इसलिए यह गैर-स्थिरता के संदर्भ में तीव्रता और अवधि की संयुक्त विशेषताओं का अध्ययन करने के लिए महत्वपूर्ण है, खासकर शहरी क्षेत्रों में जहां संबंध अधिक अलग हैं। इसलिए, समय-बदलती बहु-विविधता संभावना विश्लेषण समय-बदलती तीव्रता-अवधि के संबंध को प्राप्त करने के लिए कार्यान्वित किया जाता है। डिफरेंशियल इवोल्यूशन मार्कोव चेन (डीई-एमसी) एल्गोरिथ्म के माध्यम से बायेसियन दृष्टिकोण समय-भिन्न रिटर्न स्तर के अनिश्चितता के अनुमान का अनुमान लगाने के लिए कार्यरत है। परिणाम इस बात पर जोर देते हैं कि संभाव्यता वितरण पैरामीटर अस्थायी और स्थानिक रूप से भिन्न होते हैं और चरम घटना मॉडलिंग में गैर-स्थैतिकता को शामिल करने की सलाह देते हैं यदि संभाव्यता वितरण मापदंडों में बदलाव होता है। यह गैर-स्थिर मॉडल पारंपरिक स्थिर / गैर-प्राथमिक तरीकों की तुलना में बेहतर सटीकता और विश्वसनीयता के साथ रिटर्न स्तर की गणना करने के लिए मूल रूप से नियोजित किया जा सकता है। परिणाम बताते हैं कि लंबी अवधि के रिटर्न स्तर की तुलना में बड़ी अवधि की विश्वसनीयता अंतराल के साथ, छोटी अवधि की वापसी का स्तर लंबे लोगों की तुलना में तेज दर से बढ़ता है। परिणाम जल संसाधन प्रणालियों के डिजाइन के लिए घटना आधारित गैर-स्थिर आईडीएफ घटना को अपनाने और बदलते जलवायु के प्रभावों को दूर करने के लिए दीर्घकालिक निर्णय लेने की रणनीतियों को तैयार करने के महत्व को भी उजागर करते हैं।

सूखे पर हालिया साहित्य सूखे की विशेषताओं के गतिशील व्यवहार को शामिल करते हुए सूखा सूचकांक विकसित करने की आवश्यकता पर जोर देता है। इसलिए, बहु-स्थिर गैर-स्थिर सूखा सूचकांक, जिसे गैर-स्थिर संयुक्त घाटा सूचकांक (NJDI) के रूप में कहा जाता है, को हाइड्रोलॉजिकल चर के अस्थायी गतिशीलता को पकड़ने और भारत के मौसम संबंधी सूखाग्रस्त क्षेत्रों की पहचान करने के लिए विकसित किया गया है। वर्षा श्रृंखला के वितरण पैरामीटर में देखे गए परिवर्तन पूरे पूर्वोत्तर में छोड़कर पूरे भारत में हाल के दशकों में शुष्क दिनों की बढ़ती संख्या पर जोर देते हैं। एनजेडीआई और स्थिर जॉइंट डेफिसिट इंडेक्स (जेडीआई) की तुलना से पता चलता है कि जेडीआई सूखे को कम कर देता है जब लगातार गंभीर सूखा घटनाओं का क्लस्टर होता है और इसके विपरीत होता है। यह स्पष्ट रूप से दर्शाता है कि पारंपरिक सूचकांक वर्षा की सबसे कम परिमाण द्वारा पक्षपाती हैं। इसके अतिरिक्त, NJDI और JDI के ऐतिहासिक सूखे के

आकलन के स्थानिक बदलाव स्पष्ट रूप से दर्शाते हैं कि अधिकांश क्षेत्रों में, JDI ने 19 वीं सदी की शुरुआत में सूखे को कम करके आंका था और सदी के बाद के हिस्से में इसे ज़्यादा करके आंका, जो कि परिवर्तनों में सामंजस्य के साथ है। भारत पर शुष्क घटनाओं का पैटर्न, जबकि, एनजेडीआई ने ऐतिहासिक सूखा पर कब्जा कर लिया, जो वर्षा श्रृंखला की लौकिक गतिशीलता को दर्शाता है और पारंपरिक सूखे सूचकांकों की तुलना में अधिक विश्वसनीय है। प्रस्तावित एनजेडीआई को गैर-जलवायु में सूखे की निगरानी के लिए एक संभावित सूचकांक के रूप में पाया जाता है।

अंत में, प्रस्तावित TSW-NSM को कोवरेट के रूप में जलवायु चर को अपनाकर और बेहतर किया जाता है। हाल के अध्ययनों ने एक कोवरिएट के रूप में समय की उपयुक्तता पर सवाल उठाया है और जलवायु-सूचित कोवरिएट को शामिल करके मॉडल की सटीकता में सुधार की संभावना पर जोर दिया है। गैर-प्राथमिक वार्षिक अधिकतम वर्षा और तीव्रता श्रृंखला को मॉडल करने के लिए पांच संभावित जलवायु-सूचित कोवरियेट को चुना गया है। वितरण मापदंडों में परिवर्तन TSW का उपयोग करके पता लगाया जाता है, और मॉडल के 32 संयोजन विकसित किए जाते हैं। इसके अलावा, बेयसियन डिफरेंशियल इवोल्यूशनरी मोटे कार्लो (डीई-एमसी) एल्गोरिथ्म को गैर-स्थिर मापदंडों की अनिश्चित सीमा का अनुमान लगाने के लिए नियोजित किया गया है, और सबसे अच्छे मॉडल को डीविनस सूचना मानदंड (डीआईसी) का उपयोग करके चुना गया है। यह बताता है कि छोटी अवधि की तीव्रता की घटनाएं स्थानीय प्रक्रियाओं (यानी, स्थानीय तापमान में परिवर्तन और पूर्ण तापमान में परिवर्तन) से अधिक प्रभावित होती हैं, जबकि लंबी अवधि की तीव्रता की घटनाएं वैश्विक प्रक्रियाओं (ग्लोबल वार्मिंग और टेलीकनेक्ट्स) से प्रभावित होती हैं। हालांकि, स्वीकार्य गैर-स्थिर मॉडल से पता चलता है कि तापमान-आधारित सहसंयोजक, अर्थात्, स्थानीय, पूर्ण और वैश्विक तापमान में परिवर्तन, गतिशील व्यवहार को पकड़ने में हमेशा अच्छा रहा है। यह भी देखा गया है कि स्थानीय प्रक्रियाएं वैश्विक प्रक्रियाओं के हस्ताक्षर को ले जाती हैं। इसके अलावा, सबसे अच्छा गैर-स्थिर मॉडल के माध्यम से गणना की गई रिटर्न स्तर दिखाता है कि वापसी की अवधि कम हो रही है, और छोटी अवधि की घटनाओं में लंबी अवधि की घटनाओं की तुलना में भारी बदलाव आया है। इसके अलावा, बदलती जलवायु के प्रभावों को दूर करने के लिए दीर्घकालिक रणनीतियों को तैयार करने के लिए जलवायु-आधारित सहसंयोजकों पर आधारित गैर-केंद्रित मॉडलिंग को अपनाना आवश्यक है।

यह उम्मीद की जाती है कि भारत में वर्षा और तापमान में हुए ऐतिहासिक बदलावों की मात्रा का निर्धारण क्षेत्रीय अनुकूलन रणनीतियों को लागू करने में मदद कर सकता है। बहुभिन्नरूपी अप्रत्यक्ष चरम घटना मॉडलिंग का प्रस्तावित ढांचा इस अध्ययन में उल्लिखित अनुप्रयोगों तक ही सीमित नहीं है। यह

सामान्य है और इसे किसी भी जलवायु मॉडलिंग में नियोजित किया जा सकता है जो गैर-स्थिरता के हस्ताक्षर को प्रदर्शित करता है।

# CONTENTS

Certificate.....	i
Acknowledgments .....	iii
Abstract.....	v
संसार.....	ix
List of Figures.....	xix
List of Tables .....	xxix
Abbreviations.....	xxxix
1 Introduction.....	1
1.1 Background.....	1
1.2 Nonstationary Extreme Value Analysis.....	3
1.2.1 Univariate Analysis.....	3
1.2.2 Multivariate Analysis.....	4
1.3 Motivation.....	5
1.4 Objectives .....	7
1.5 Organization of the Thesis .....	7
2 Changing Characteristics of Extreme Wet and Dry Spells of Indian Monsoon Rainfall .....	9
2.1 Introduction.....	9
2.2 Data Used and Study Region .....	10
2.3 Methodology .....	15
2.3.1 Extraction of Extreme Wet and Dry Spells .....	15
2.3.2 Trend Analysis and Testing of Significance.....	17
2.4 Results and Discussion .....	18
2.4.1 Spatio-temporal Variation of Extremes Days and Spells .....	20
2.4.2 Spatio-temporal Variation of Accumulated Depth and Spell Length .....	23
2.5 Examination of Shifts in Spatio-temporal Rainfall Patterns.....	29
2.6 Physical Interpretation .....	32
2.7 Concluding Remarks.....	33
3 Unraveling Diurnal Asymmetry of Surface Temperature in Different Climate Zones .....	37
3.1 Introduction.....	37
3.2 Data Description .....	39
3.3 Methodology .....	39
3.3.1 Extreme Event Indices .....	39
3.3.2 Multidimensional Ensemble Empirical Mode Decomposition.....	40
3.3.2.1 Empirical Mode Decomposition.....	40
3.3.2.2 Ensemble Empirical Mode Decomposition .....	41
3.3.2.3 Test for Significance .....	43

3.4	Results and Discussion .....	43
3.4.1	Variations in the EEMD Trends of DTR, $T_{\max}$ , and $T_{\min}$ .....	44
3.4.1.1	Annual Variations .....	44
3.4.1.2	Seasonal Variations.....	46
3.4.2	Extremes of $T_{\max}$ and $T_{\min}$ .....	49
3.4.3	Influence of Regional Climate on DTR.....	52
3.4.4	Physical Interpretation .....	54
3.5	Concluding Remarks.....	56
4	Quantifying the Shifts and Intensification in the Annual Cycles of Diurnal Temperature Extremes for Human Comfort and Crop Production .....	59
4.1	Introduction.....	59
4.2	Data and Methods .....	61
4.2.1	Data Description .....	61
4.2.2	Growing Season and Transition Period .....	61
4.2.3	Extraction of Indices and their Trend .....	62
4.3	Results and Discussion .....	63
4.3.1	Joint Behavior of Diurnal Extremes .....	65
4.3.2	Changes in the Growing Season .....	69
4.3.3	Changes in the Transition Period.....	73
4.4	Concluding Remarks.....	75
5	Bringing Realism into a Dynamic Copula-Based Nonstationary Intensity-Duration Model .....	77
5.1	Introduction.....	77
5.2	Data and Methodology.....	78
5.2.1	Study Area and Data Description .....	78
5.3	Methodology .....	79
5.3.1	Definition and Extraction of Storm Events.....	81
5.3.2	Marginal Distribution of Storm Events and its Dependence Structure .....	81
5.3.3	Detection of Non-stationarity .....	83
5.3.4	Parameter Estimation using Bayesian Inference.....	85
5.3.5	Return Level and Return Period .....	88
5.4	Results and Discussion .....	89
5.4.1	Extraction of storm attributes and its distribution.....	90
5.5	Detecting and Estimating Nonstationary Parameters.....	92
5.6	Estimation of Time-Varying Parameters using Bayesian Inference .....	96
5.7	Time-varying Bivariate Frequency Analysis .....	105
5.8	Concluding Remarks.....	114
6	A Copula-based Nonstationary Joint Deficit Index for Droughts.....	117
6.1	Introduction.....	117
6.2	Study Area and Data Description.....	119
6.3	Methodology .....	119
6.3.1	Modified Standardized Index and its Marginal Distribution .....	120
6.3.2	Detection of Non-stationarity .....	120
6.3.3	Nonstationary Joint Drought Index.....	122
6.4	Results and Discussion .....	123

6.4.1	Extraction of Marginals .....	123
6.4.2	Detection and Estimation of Nonstationary Parameters .....	124
6.4.3	Nonstationary Joint Deficit Index .....	131
6.5	Concluding Remarks.....	137
7	Refining the Intensity-Duration-Frequency Curve Relationships through Climate-informed Covariates.....	139
7.1	Introduction.....	139
7.2	Data Description .....	140
7.3	Methodology .....	142
7.3.1	Nonstationary Extreme Event Model .....	143
7.3.2	Construction of Nonstationary IDF curves.....	148
7.4	Results and Discussion .....	148
7.4.1	Nonstationary Extreme Event Model .....	148
7.4.2	Detecting and Estimating Nonstationary Parameters .....	149
7.4.3	Selection of best covariate .....	152
7.4.4	Nonstationary IDF curves.....	163
7.5	Concluding Remarks.....	169
8	Summary and Recommendations.....	171
8.1	Summary .....	171
8.2	Recommendations for Future Work.....	174
	References.....	177
A	Annexure I.....	195
B	Publications and Achievements .....	209
B.1	Journal Publications .....	209
B.2	Conference Publications .....	209
B.3	Awards/Achievements .....	210
C	Vitae .....	211

## LIST OF FIGURES

Figure 1.1: Illustration of the effect of the shift in mean and variance.....	2
Figure 2.1: a) Spatial distribution of the mean annual rainfall (mm/day) for the period 1901 to 2013 and b) Homogenous monsoon rainfall regions of India, as defined by IITM. ....	15
Figure 2.2: Annual maximum daily rainfall intensity a) Average (in mm) for 1901 to 2013, b) Spatial Variance over India; S1 and S2 indicates the linear trend for 1901 to 1950 and 1951 to 2013 respectively, and ‘*’ denotes significant trend, c) Box plots corresponding to the spatial variance for each 10 year period, d) Long Term Trend (Positive and Negative) for 1901 to 2013. ....	19
Figure 2.3: Spatial time varying trend of annual maximum intensity for three 50 year windows a) initial - 1901 to 1950, b) middle - 1931 to 1980 and c) final - 1961 to 2010. ....	20
Figure 2.4: a) Long term trend for $N_{WD}$ ; b) Long term trend for $F_{WS}$ ; c) Time-varying trend in terms of number of grids for $N_{WD}$ and $F_{WS}$ ; d) Long term trend for $N_{DD}$ ; e) Long term trend for $F_{DS}$ ; f) Time-varying trend in terms of number of grids for $N_{DD}$ and $F_{DS}$ .....	21
Figure 2.5: Spatial time-varying trend of $N_{WD}$ (top panel) for three 50 year windows a) initial - 1901 to 1950, b) middle - 1931 to 1980 and c) final - 1961 to 2010. Spatial time-varying trend of $F_{WS}$ (bottom panel) for three 50-year windows d) initial - 1901 to 1950, e) middle - 1931 to 1980 and f) final - 1961 to 2010. ....	22
Figure 2.6: Spatial time-varying trend of $N_{DD}$ (top panel) for three 50 year windows a) initial - 1901 to 1950, b) middle - 1931 to 1980 and c) final - 1961 to 2010. Spatial time-varying trend of $F_{DS}$ (bottom panel) for three 50-year windows d) initial - 1901 to 1950, e) middle - 1931 to 1980 and f) final - 1961 to 2010. The pie chart shows the percentage of the significant trend at 10% significance level, which corresponds to a 90% confidence interval. ....	23
Figure 2.7: Temporal mean of a) $AD_{WS}$ in mm b) $AL_{WS}$ and c) $AL_{DS}$ for 1901 to 2013; Long term trend of d) $AD_{WS}$ , e) $AL_{WS}$ and f) $AL_{DS}$ , for 1901 to 2013. The pie chart shows the statistical trend at 10% significance level; Time-varying trend of g) $AD_{WS}$ , h) $AL_{WS}$ , and i) $AL_{DS}$ , for 50 year moving window with a 10 year difference. ....	24
Figure 2.8: Temporal mean of a) $MD_{WS}$ in mm, b) $ML_{WS}$ and c) $ML_{DS}$ in days, for 1901 to 2013; Long term trend of d) $MD_{WS}$ , e) $ML_{WS}$ and f) $ML_{DS}$ , for 1901 to 2013. The pie chart shows the statistical trend at 10% significance level; Time-varying trend of g) $MD_{WS}$ , h) $ML_{WS}$ , and i) $ML_{DS}$ , for 50 year moving window with 10 year difference. ....	25
Figure 2.9: Spatial time-varying trend of $AD_{WS}$ (top panel) for three 50 year windows a) initial - 1901 to 1950, b) middle - 1931 to 1980 and c) final - 1961 to 2010. Spatial time-varying trend of $AL_{WS}$ (bottom panel) for three 50-year windows d) initial - 1901 to 1950, e) middle - 1931 to 1980 and f) final - 1961 to 2010.	

The pie chart shows the percentage of the significant trend at 10% significance level, which corresponds to a 90% confidence interval. ....26

Figure 2.10: Spatial time-varying trend of  $MD_{WS}$  (top panel) for three 50 year windows a) initial - 1901 to 1950, b) middle - 1931 to 1980 and c) final - 1961 to 2010. Spatial time-varying trend of  $ML_{WS}$  (bottom panel) for three 50-year windows d) initial - 1901 to 1950, e) middle - 1931 to 1980 and f) final - 1961 to 2010. ....27

Figure 2.11: Similarity between the  $AD_{WS}$  and  $AL_{WS}$  a) 50 year moving window with 10 year difference and b) spatial plot of last 50 year window. Grouping is done into eight baskets, (A) No trend in  $AD_{WS}$  and positive trend in  $AL_{WS}$ , (B) No trend in  $AD_{WS}$  and negative trend in  $AL_{WS}$ , (C) Positive trend in  $AD_{WS}$  and no trend in  $AL_{WS}$ , (D) Negative trend in  $AD_{WS}$  and no trend in  $AL_{WS}$ , (E) Positive trend in both  $AD_{WS}$  and  $AL_{WS}$ , (F) Positive trend in  $AD_{WS}$  and negative trend in  $AL_{WS}$ , (G) Negative trend in  $AD_{WS}$  and positive trend in  $AL_{WS}$ , and (H) Negative trend in both  $AD_{WS}$  and  $AL_{WS}$ . ....28

Figure 2.12: Spatial time-varying trend of  $AL_{DS}$  (top panel) for three 50 year windows a) initial - 1901 to 1950, b) middle - 1931 to 1980 and c) final - 1961 to 2010. Spatial time-varying trend of  $ML_{DS}$  (bottom panel) for three 50-year windows d) initial - 1901 to 1950, e) middle - 1931 to 1980 and f) final - 1961 to 2010. ....29

Figure 2.13: Most probable month of  $O_{WS}$  (top panel) for three 50 year windows a) initial - 1901 to 1950, b) middle - 1931 to 1980 and c) final - 1961 to 2010. Most probable month of  $O_{DS}$  (bottom panel) for three 50-year windows d) initial - 1901 to 1950, e) middle - 1931 to 1980 and f) final - 1961 to 2010. Most probable month of g)  $O_{WS}$  and h)  $O_{DS}$  for 50 year moving window with a 10-year difference.....30

Figure 2.14:  $I_{WS}$  of 50 year Return period a) Box plot of 10 year advance time step, which explains the spatial variance over India, b) Long term trend for 1901 to 2013, c) Time-varying trend, in terms of the number of grids showing significant trend for 50 year moving window and d) Similarity diagram for the successive 50 year moving window with 10 year difference.....31

Figure 2.15: Spatial time-varying trend for 50 year return level for three 50 year windows a) initial - 1901 to 1950, b) middle - 1931 to 1980 and c) final - 1961 to 2010. The pie chart shows the percentage of the significant trend at 10% significance level, which corresponds to a 90% confidence interval. ....32

Figure 2.16: Daily mean temperature trend for 1951 to 2013. The pie chart shows the percentage of the significant trend at 10% significance level, which corresponds to a 90% confidence interval. ....33

Figure 3.1: Steps involved in Ensemble Empirical Mode Decomposition of a time series. ....42

Figure 3.2: a) Annual variation of spatially averaged annual temperature over India and b) Average DTR from 1951 to 2010. Grids with inconsistent data are shown in grey color (extreme bottom of color bar), which is represented as NA (Not Analyzed). ....44

Figure 3.3: Spatial evolution of Ensemble Empirical Mode Decomposition trend of annual a) DTR, b) Maximum and c) Minimum temperatures. Each sub-panel has four time windows 1) 1951-1980, 2) 1951-1990, 3) 1951-2000 and 4) 1951-2010. ....	45
Figure 3.4: Spatial evolution of Ensemble Empirical Mode Decomposition trend of seasonal DTR for a) DJF, b) MAM, c) JJA and d) SON. Each sub-panel has four time windows 1) 1951-1980, 2) 1951-1990, 3) 1951-2000 and 4) 1951-2010.....	46
Figure 3.5: Spatial evolution of Ensemble Empirical Mode Decomposition trend of seasonal maximum temperature for a) DJF, b) MAM, c) JJA and d) SON. Each sub-panel has four windows 1) 1951-1980, 2) 1951-1990, 3) 1951-2000 and 4) 1951-2010.. ....	48
Figure 3.6 Spatial evolution of Ensemble Empirical Mode Decomposition trend of seasonal minimum temperature DTR for a) DJF, b) MAM, c) JJA and d) SON. Each sub-panel has four windows 1) 1951-1980, 2) 1951-1990, 3) 1951-2000 and 4) 1951-2010.....	49
Figure 3.7: Ensemble Empirical Mode Decomposition trend of a) SU (days), b) TX10p (days) c) TX90p (days) and d) WSDI (days). Each sub-panel has four windows 1)1951-1980, 2)1951-1990, 3)1951-2000 and 4)1951-2010.....	50
Figure 3.8: Ensemble Empirical Mode Decomposition trend for the annual occurrence of a) TR (days), b) TN10p (days) c) TN90p (days) and d) CSDI (days). Each sub-panel has four windows 1)1951-1980, 2)1951-1990, 3)1951-2000 and 4)1951-2010.....	51
Figure 3.9: Scatter plot of Ensemble Empirical Mode Decomposition trend in a) positive trend of DTR and $T_{max}$ ( $T_{min}$ ) and b) negative trend of DTR and $T_{max}$ ( $T_{min}$ ) for the last time window (1951-2010). Unit is in °C. ....	52
Figure 3.10: Regional Ensemble Empirical Mode Decomposition trend of DTR, $T_{max}$ , and $T_{min}$ for heterogeneous climatic zones a) 1951-1980, b) 1951-1990, c) 1951-2000 and d) 1951-2010, e) representative grids in different climatic zones. ....	52
Figure 3.11: Statistically significant Ensemble Empirical Mode Decomposition trend of a) DTR (°C), b) average maximum temperature (°C) c) average minimum temperature (°C), d) SU (days), e) TX10p (days), f) TX90p (days), g) TR (days), h) TN10p (days), i) TN90p (days), j) WSDI (days) and k) CSDI (days) for 1951-2010 (final time window).....	53
Figure 3.12: Ensemble Empirical Mode Decomposition trend for annual sea surface temperature (°C) for the period of 1982-2010.. ....	55
Figure 4.1: Illustrative plot of typical ALC of $T_{min}$ (blue line) and $T_{max}$ (red line) and extraction of onset and termination of the growing season. ....	62
Figure 4.2: a) The 60 years (1951-2010) spatio-temporal average ALC for $T_{max}$ (red line), $T_{min}$ (blue line), and rainfall (light blue). The units are normalized. Spatial variation of the peak value of this average ALC of b) $T_{max}$ and c) $T_{min}$ . White dots in (b) and (c) represents grids exhibiting bi-modal behavior, while grids	

	without a dot represent unimodal behavior. Spatial information of the month exhibiting this peak in the average ALC of d) $T_{max}$ and e) $T_{min}$ . .....	64
Figure 4.3:	Temporal average of a) Amplitude of $T_{max}$ , b) Amplitude of $T_{min}$ , c) Month in which the amplitude of $T_{max}$ occurs and d) Month in which the amplitude of $T_{min}$ occurs. White dots in (a) and (b) represents grids exhibiting 2 modes/year, while grids without dot represent 1 mode/year. Each sub-panel has three windows, namely 1) first decade (1951-1960) 2) middle decade (1976-1985) and 3) last decade (2001-2010). .....	65
Figure 4.4:	Joint probability of $T_{max}$ and $T_{min}$ a) spatial average of ALC for entire India, b) for each panel with 5 °C increments and c) for each panel with 2 °C increment, which is the expansion of the subpanel of (b) with the spatial variation of $T_{max}$ 30 °C to 35 °C and $T_{min}$ 20 °C to 25 °C for 60 years (1951-2010).. .....	66
Figure 4.5:	Joint probability of $T_{max}$ and $T_{min}$ a) spatial average of ALC for entire India, b) for each panel with 5 °C increments and c) for each panel with 2 °C increment, which is the expansion of the subpanel of (b) with the spatial variation of $T_{max}$ 30 °C to 35 °C and $T_{min}$ 20 °C to 25 °C for the middle decade (1976-1985). .....	68
Figure 4.6:	Joint probability of $T_{max}$ and $T_{min}$ a) spatial average of ALC for entire India, b) for each panel with 5 °C increments and c) for each panel with 2 °C increment, which is the expansion of the subpanel of (b) with the spatial variation of $T_{max}$ 30 °C to 35 °C and $T_{min}$ 20 °C to 25 °C for the final decade (2001-2010). .....	69
Figure 4.7:	Average of a) OGS (days) and b) LGS (days) for 1951 to 2010, c) scatter plot of the OGS (days) and LGS (days) for the first (1951-1960), middle (1976 – 1985) and last (2001 – 2010) decades along with the respective marginal probability plots. Spatial evolution of Ensemble Empirical Mode Decomposition trends of d) OGS (days) and e) LGS (days). Each sub-panel has four windows 1) 1951-1980, 2) 1951-1990, 3) 1951-2000 and 4) 1951-2010. ....	70
Figure 4.8:	Temporal average of a) OGS b) LGS, c) TWS and d) TSW. Each sub-panel has three windows, namely 1) first decade (1951-1960) 2) middle decade (1976-1985) and 3) last decade (2001-2010). .....	71
Figure 4.9:	Spatial evolution of Ensemble Empirical Mode Decomposition trend of a) onset of extreme summer (when $T_{max} \geq 35$ °C and $T_{min} \geq 25$ °C), b) Total number of days in extreme summer and c) total number of days in winter (when $T_{max} \leq 25$ °C and $T_{min} \leq 10$ °C). Each sub-panel has four windows 1) 1951-1980, 2) 1951-1990, 3) 1951-2000 and 4) 1951-2010. ....	73
Figure 4.10:	Average of a) Transition period of winter to summer ( $T_{ws}$ ) in days and b) Transition period of summer to winter ( $T_{sw}$ ) in days for 1951 to 2010, b) scatter plot of the $T_{ws}$ (days) and $T_{sw}$ (days) for the first (1951-1960), middle (1976 – 1985) and last (2001 – 2010) decade along with the respective marginal probability plots. Spatial evolution of the Ensemble Empirical Mode Decomposition trend of d) $T_{ws}$ (days) and e) $T_{sw}$ (days). Each sub-	

panel has four windows 1) 1951-1980, 2) 1951-1990, 3) 1951-2000 and 4) 1951-2010. ....	74
Figure 5.1: Steps involved in the nonstationary intensity-duration model. ....	80
Figure 5.2: Comparison of the traditional nonstationary method and the proposed time-sliding window approach. ....	85
Figure 5.3: Trends in the time series (first column) and parameters series (second and third columns) for the four synthetic series generated.....	90
Figure 5.4: Scatter plot of storm intensity vs. storm duration along with their marginal distributions for a) Bangalore, b) Bombay, c) Calcutta and d) Madras. ....	92
Figure 5.5: Parameters of distribution computed using time sliding window series and their trend for Bangalore. ....	93
Figure 5.6: Same as Figure 5.5, but for Bombay station. ....	93
Figure 5.7: Same as Figure 5.5, but for Calcutta station. ....	94
Figure 5.8: Same as Figure 5.5, but for Madras station.....	94
Figure 5.9: Trace plots (left panel) and posterior density plots (right panel) for the posterior samples of the linear nonstationary model of storm duration for Bangalore. ....	98
Figure 5.10: Posterior distribution of marginals using stationary parameters for Bangalore .....	99
Figure 5.11: Posterior distribution of marginals using nonstationary parameters for Bangalore .....	99
Figure 5.12: Posterior distribution of marginals using stationary parameters for Bombay .....	100
Figure 5.13: Posterior distribution of marginals using nonstationary parameters for Bombay .....	100
Figure 5.14: Posterior distribution of marginals using stationary parameters for Calcutta .....	101
Figure 5.15: Posterior distribution of marginals using nonstationary parameters for Calcutta .....	101
Figure 5.16: Posterior distribution of marginals using stationary parameters for Madras .....	102
Figure 5.17: Posterior distribution of marginals using stationary parameters for Madras .....	102
Figure 5.18: RL of storm intensity (left panel) and storm duration (right panel) for 10, 30 and 100-year events for a) Bangalore, b) Bombay, c) Calcutta and d) Madras. ....	105
Figure 5.19: Joint return period (year) of storm intensity (mm/hr) and storm duration (hr) for a) Bangalore, b) Bombay, c) Calcutta and d) Madras using the median value of the posterior distribution of sample parameters. ....	106
Figure 5.20: Evolution of return period (year) over time for the maximum flood intensity for 1 hr, 48 hr and maximum duration of the storm event extracted from the observed data for a) Bangalore, b) Bombay and c) Madras respectively. .	107

Figure 5.21. Evolution of return period (year) over time for the selected major flood intensity having duration 24h, 24h and 12h for a) Bangalore, b) Bombay and c) Madras respectively. ....108

Figure 5.22: IDF curve for Bangalore: a) nonstationary average IDF curve for a 100-year event with their uncertainty bound of 90% credible interval. The black dots represent the median value of the stationary average IDF curve, whose uncertainty bound is not shown here. The inset plot shows the time-varying RL of 1 hr (red line), 24 hr (pink line) and 49 hr (green line) event, b) nonstationary vs. stationary RL for 1 hr duration, boxplot represents nonstationary and green ‘\*’ represents stationary RL and c) Difference between nonstationary and stationary RL for 1 hr duration.....109

Figure 5.23: IDF curve for Bombay: a) nonstationary average IDF curve for a 100-year event with their uncertainty bound of 90% credible interval. The black dots represent the median value of the stationary average IDF curve. The inset plot shows the time-varying RL of 1 hr (red line), 24 hr (pink line) and 49 hr (green line) event, b) nonstationary vs. stationary RL for 1 hr duration, boxplot represents nonstationary and green ‘\*’ represents stationary RL and c) Difference between nonstationary and stationary RL for 1 hr duration.110

Figure 5.24: IDF curve for Calcutta: a) nonstationary average IDF curve for a 100-year event with their uncertainty bound of 90% credible interval. The black dots represent the median value of the stationary average IDF curve, whose uncertainty bound is not shown here. The inset plot shows the time-varying RL of 1 hr (red line), 24 hr (pink line) and 49 hr (green line) event, b) nonstationary vs. stationary RL for 1 hr duration, boxplot represents nonstationary and green ‘\*’ represents stationary RL and c) Difference between nonstationary and stationary RL for 1 hr duration.....111

Figure 5.25: IDF curve for Madras: a) nonstationary average IDF curve for a 100-year event with their uncertainty bound of 90% credible interval. The black dots represent the median value of the stationary average IDF curve. The inset plot shows the time-varying RL of 1 hr (red line), 24 hr (pink line), and 49 hr (green line) event. b) nonstationary vs. stationary RL for 1 hr duration, boxplot represents nonstationary and green ‘\*’ represents stationary RL and c) Difference between nonstationary and stationary RL for 1 hr duration.112

Figure 5.26: Difference between nonstationary and stationary return level for different return period for 1 hr duration of a) Bangalore, b) Bombay, c) Calcutta and d) Madras .....112

Figure 5.27: Nonstationary (left column) and stationary (right column) average IDF curve for different return periods of a) Bangalore, b) Bombay, c) Calcutta and d) Madras.....113

Figure 6.1: Comparison between conventional and modified 1-month SI for grid location of 26 °N and 93 °E: a) monthly rainfall of 1965; Red line in the upper panel (a) represents the average rainfall of each month for the period of 1901 to 2013; b) conventional SI of each month; and c) modified SI of each month. ....124

Figure 6.2: a) Parameters (alpha and beta) of gamma distribution computed using time sliding window series and their change point, b) mean and variance of gamma distribution and their change point. Nonstationary modeling of precipitation for grid location 21.5 °N and 79.25 °E c) without change point, d) the respective change point of $\alpha$ and $\beta$ are considered, e) change point of $\alpha$ is considered for both $\alpha$ and $\beta$ , f) change point of $\beta$ is considered for both $\alpha$ and $\beta$ g) change point in the mean is considered as a change point for $\alpha$ and $\beta$ , and h) change point variance is considered for $\alpha$ and $\beta$ . the light grey, dark grey and black region represents the area between the 0.05 to 0.95, 0.25 to 0.75 and 0.5 quantiles; while the red dots indicate the observed values .....	127
Figure 6.3: Spatial variation of nonstationary parameters for June at 1 month time scale. The top panel shows the trend in $\alpha$ parameter, and the bottom panel shows trend in $\beta$ parameter, (a) without change point, (b) before change point and (c) after the change point. ....	128
Figure 6.4: Same as Figure 6.3 for July .....	129
Figure 6.5: Same as Figure 6.3 for August .....	129
Figure 6.6: Same as Figure 6.3 for September .....	130
Figure 6.7: Non-stationarity in the rainfall series of September -1 month time scale for location 96 (left panel) and 3372 (right panel). a) parameter series of $\alpha$ and its trend, b) parameter series of $\beta$ and its trend and c) PDF of rainfall depth. ....	131
Figure 6.8: Historical drought classification of 3 month time scale rainfall depth of September for the period of 1902 to 2013 using modified a) NSI and b) SI at grid location of 10.5 °N, 78 °E. ....	132
Figure 6.9: Historical drought classification of 6 month time scale rainfall depth of September for the period of 1902 to 2013 using modified a) NSI and b) SI at grid location of 10.5 °N, 78 °E. ....	133
Figure 6.10: Historical drought classification of 3 month time scale rainfall depth of September for the period of 1902 to 2013 using modified a) NSI and b) SI at grid location of 26.5 °N, 72.75 °E. ....	133
Figure 6.11: Historical drought classification of 6 month time scale rainfall depth of September for the period of 1902 to 2013 using modified a) NSI and b) SI at grid location of 26.5 °N, 72.75 °E. ....	134
Figure 6.12: Spatial comparison of drought classification between NJDI and JDI for a) Sep 1918, b) Sep 1920 and c) Sep 1941 .....	135
Figure 6.13: Spatial comparison of drought classification between NJDI and JDI for a) Sep 1965, b) Sep 1987 and c) Sep 2002 .....	136
Figure 6.14: Spatial comparison of drought classification between NJDI and JDI for 1918 (first two panels) and 2002 (last two panels) of a) June, b) July, c) August, d) September and e) October.....	137
Figure 7.1. Steps involved in developing nonstationary IDF curve .....	143
Figure 7.2: Boxplots of annual maximum intensity rainfall of each duration for a) Bangalore, b) Bombay, c) Calcutta and d) Madras.....	149

Figure 7.3: Trace plots (left panel) and posterior density plots (right panel) for the posterior samples of the linear nonstationary model of 1 hr duration rainfall intensity for Bangalore.....	151
Figure 7.4: CDFs of Bangalore station for a) 2hr, b) 3hr, c) 6hr, d) 12hr, e) 18hr and f) 48hr duration rainfall. The dark blue line represents the best time-varying model for extreme rainfall intensities, and CL represents its credible limit. The acceptable models are within the credible limit of the best model.....	154
Figure 7.5: CDFs of Bombay station for a) 2hr, b) 3hr, c) 6hr, d) 12hr, e) 18hr and f) 48hr. The dark blue line represents the best time-varying model for extreme rainfall intensities, and CL represents its credible limit. The acceptable models are within the credible limit of the best model. ....	158
Figure 7.6: CDFs of Calcutta station for a) 6hr, b) 12hr, c) 18hr and d) 48hr. The dark blue line represents the best time-varying model for extreme rainfall intensities, and CL represents its credible limit. The acceptable models are within the credible limit of the best model. ....	159
Figure 7.7: CDFs Madras station for a) 2hr, b) 3hr, c) 6hr, d) 12hr and e) 18hr. The dark blue line represents the best time-varying model for extreme rainfall intensities, and CL represents its credible limit. The acceptable models are within the credible limit of the best model. ....	160
Figure 7.8: The PP for the best fitted time-varying model of each duration annual maximum rainfall series of a) Bangalore, b) Bombay, c) Calcutta and d) Madras.....	161
Figure 7.9: The QQ for the best fitted time-varying model of each duration annual maximum rainfall series of a) Bangalore, b) Bombay, c) Calcutta and d) Madras.....	162
Figure 7.10: The PDF plots for the best fitted nonstationary model of 6hr duration annual maximum rainfall series of a) Bangalore, b) Bombay, c) Calcutta and d) Madras. Red color represents the best model, and black color represents the stationary model.....	163
Figure 7.11: Nonstationary return level with its uncertainty bounds for different durations and different return period of a) 2yr, b) 5yr, c) 10yr, d) 25yr, e) 50yr and f) 100yr in Bombay station.....	164
Figure 7.12: The difference between nonstationary and stationary return level with its uncertainty bounds for different durations and different return periods in Bombay.....	165
Figure 7.13: Nonstationary return level with its uncertainty bounds for different durations and different return period of a) 2yr, b) 5yr, c) 10yr, d) 25yr, e) 50yr and f) 100yr in Bangalore station.....	166
Figure 7.14: Nonstationary return level with its uncertainty bounds for different durations and different return period of a) 2yr, b) 5yr, c) 10yr, d) 25yr, e) 50yr and f) 100yr in Calcutta station.....	166
Figure 7.15: Nonstationary return level with its uncertainty bounds for different durations and different return period of a) 2yr, b) 5yr, c) 10yr, d) 25yr, e) 50yr and f) 100yr in Madras station.....	167

Figure 7.16: The difference between nonstationary and stationary return level with its uncertainty bounds for different durations and different return periods in Bangalore. ....	167
Figure 7.17: The difference between nonstationary and stationary return level with its uncertainty bounds for different durations and different return periods in Calcutta. ....	168
Figure 7.18: The difference between nonstationary and stationary return level with its uncertainty bounds for different durations and different return periods in Madras.....	168
Figure 7.19: Difference between nonstationary and stationary return level for different return periods of 1hr duration of a) Bangalore, b) Bombay, c) Calcutta and c) Madras.....	169

## LIST OF TABLES

Table 2.1: Summary of past studies conducted on the characteristics of Indian rainfall	12
Table 2.2: Indices adopted to define various characteristics of extreme spells .....	17
Table 3.1: Climate Extreme Indices .....	40
Table 4.1: Definition of indices to identify the effect of temperature on productive elements .....	62
Table 5.1: Details of rainfall data for all four stations .....	79
Table 5.2: Details of eight probabilistic distributions considered and their parameters.	82
Table 5.3: Comparison between traditional-NSM and TSW-NSM.....	90
Table 5.4: Characteristics of Storm Attributes .....	91
Table 5.5: Details of best-fitted distributions and the trend patterns of parameter sets, along with the significance levels for all four stations .....	91
Table 5.6: Comparison between traditional-NSM and TSW-NSM (Here NS denotes non-stationarity) .....	96
Table 5.7: Nonstationary model and its time-varying parameter statistics for each station using Bayesian Inference .....	103
Table 6.1: Drought classification based on the SI values .....	123
Table 6.2: Nonstationary parameter statistics for two chosen grids using Bayesian Inference and linear fit estimate.....	126
Table 7.1. Stationary model (M1), and different nonstationary models used in the risk framework. The nonstationary models are developed through different combinations of time and five physical processes as covariates of the location and the scale parameters. ....	145
Table 7.2: Details of the trend patterns of the parameter set, along with its significance level.....	150
Table 7.3: Time-varying GEV model performance for 1hr of annual maximum rainfall series, models are sorted from lower to higher value of DIC .....	155
Table 7.4: Best Time-varying model for all durations and all stations.....	157
Table A.1: Time-varying GEV model performance for 2hr of annual maximum rainfall series, models are sorted from lower to higher value of DIC .....	195
Table A.2: Time-varying GEV model performance for 3hr of annual maximum rainfall series, models are sorted from lower to higher value of DIC .....	197
Table A.3: Time-varying GEV model performance for 6hr of annual maximum rainfall series, models are sorted from lower to higher value of DIC .....	199
Table A.4: Time-varying GEV model performance for 12hr of annual maximum rainfall series, models are sorted from lower to higher value of DIC .....	201
Table A.5: Time-varying GEV model performance for 18hr of annual maximum rainfall series, models are sorted from lower to higher value of DIC .....	203
Table A.6: Time-varying GEV model performance for 24hr of annual maximum rainfall series, models are sorted from lower to higher value of DIC .....	205
Table A.7: Time-varying GEV model performance for 48hr of annual maximum rainfall series, models are sorted from lower to higher value of DIC .....	207

## ABBREVIATIONS

ALC	Annual cycle and its Longer timescale Components
AMS	Annual Maximum Series
AVHRR	Advanced Very High-Resolution Radiometer
BIC	Bayesian Information Criterion
CDF	Cumulative Distribution Function
CL	Credible Interval
CNE	Central North East
<i>CSDI</i>	Cold spell duration index
DE-MC	Differential Evolution Markov Chain
DIC	Deviance Information Criterion
DJF	December to February
DMI	Dipole Mode Index
DTR	Diurnal Temperature Range
<i>D<sub>ws</sub></i>	Accumulated rainfall depth in each extreme wet spell
EMI	ENSO Modoki Index
ENSO	El-Niño- Southern Oscillation
ETCCDI	Expert Team on Climate Change Detection and Indices
FD	Number of Frost Days
FDF	Flood-Duration-Frequency
<i>F<sub>DS</sub></i>	Frequency (number of occurrences) of extreme dry spells in a year
<i>F<sub>ws</sub></i>	Frequency (number of occurrences) of extreme wet spells in a year
GEV	Generalized Extreme Value Distribution
GP	Generalized Pareto Distribution
GSL	Growing Season Length
GTA	Global Temperature Anomaly
HR	Hilly Region
ID	Number of Icing Days
IDF	Intensity-Duration-Frequency
IDW	Inverse Distance Weighted
IID	Independent and Identically Distributed random variables
IITM	Indian Institute of Tropical Meteorology

IMD	Indian Meteorological Department
IMF	Intrinsic Mode Functions
IOD	Indian Ocean Dipole
IPCC	Intragovernmental Panel of Climate Change
IQR	Interquartile range
ISMR	Indian Summer Monsoon Rainfall
$I_{ws}$	Maximum Intensity of each extreme wet spell
JDI	Joint Deficit Index
JJA	June to August
K-S test	Kolmogorov Smirnov test
$L_{DS}$	Length of each extreme dry spell
$L_{GS}$	Length of Growing Season
LTA	Local Temperature Anomaly
$L_{ws}$	Length of each extreme wet spell
MAM	March to May
MCMC	Monte Carlo Markov Chain
MEEMD	Multidimensional Ensemble Empirical Mode Decomposition
MK	Mann-Kendall test
MLE	Maximum Likelihood Estimate
MSDI	Multivariate Standardized Drought Index
NCC	National Climatic Centre
$N_{DD}$	Number of extreme dry days in a year
NE	North East
NJDI	Non-stationary Joint Deficit Index
$NSI^{mod}$	Modified Non-stationary Standardized Index
NSM	Non-Stationary Model
NW	North West
$N_{WD}$	Number of extreme wet days in a year
$O_{DS}$	Onset (Starting period) of each extreme dry spell
$O_{GS}$	Onset of Growing Season
$O_{ws}$	Onset (Starting period) of each extreme wet spell
PDF	Probability Density Function
PI	Peninsular India
POT	Peak Over Threshold

RL	Return Level
RMSE	Root Mean Square Error
SDF	Severity-Duration-Frequency
SI <sup>mod</sup>	modified Standardized Index
SOI	Southern Oscillation Index
SON	September to November
SPEI	Standardized Precipitation Evapotranspiration Index
SPI	Standardized Precipitation Index
SRI	Standardized Runoff Index
SSI	Standardized Soil moisture Index
SST	Sea Surface Temperature
SSTA	Sea Surface Temperature Anomaly
<i>SU</i>	Summer days
<i>T<sub>max</sub></i>	Maximum temperature
<i>T<sub>mean</sub></i>	Mean temperature
<i>T<sub>min</sub></i>	Minimum temperature
<i>TN10p</i>	Cold nights
<i>TR</i>	Tropical nights
TSW	Time–Sliding Window approach
<i>T<sub>sw</sub></i>	Transition period of summer to winter
<i>T<sub>ws</sub></i>	Transition period of winter to summer
<i>TX10p</i>	Warm nights
<i>TX90p</i>	Warm days
WC	West Central
WG	Western Ghats
WMO	World Meteorological Organization
WSDI	Warm spell duration index